



Relation of normal load with test temperature at mild–severe wear transition state for Mg–Gd–Y–Zr alloy

Yuan-bo WANG¹, Wei ZHAO¹, Liang LI¹, Jian AN^{1,2}

1. School of Materials Science and Engineering, Jilin University, Changchun 130025, China;

2. Key Laboratory of Automobile Materials, Ministry of Education, Jilin University, Changchun 130025, China

Received 6 September 2020; accepted 8 July 2021

Abstract: The wear behavior and mild–severe (M–S) wear transition of Mg–10Gd–1.5Y–0.4Zr alloy were investigated within a temperature range of 20–200 °C. The morphologies and compositions of worn surfaces were examined to identify the wear mechanisms using scanning electron microscope and energy dispersive X-ray spectrometer. The microstructure and hardness in the subsurfaces were analyzed to reveal the M–S wear transition mechanism. Under a constant loads of 20, 35 and 40 N, each wear rate–test temperature curve presented a turning point which corresponded to the M–S wear transition. In mild wear, the surface material was plastically deformed and hence was strain-hardened, whereas in severe wear, the surface material was dynamically recrystallized and consequently was softened. It has been found that the critical temperature for M–S wear transition decreases with increasing the normal load, and the normal load exhibits an almost linear relationship with critical temperature for M–S wear transition. This work reveals that the M–S wear transition of the studied alloy conforms to the surface DRX temperature criterion.

Key words: Mg–Gd–Y–Zr alloy; elevated-temperature wear; microstructure; recrystallization; mild–severe wear transition

1 Introduction

Mg–Gd–Y–Zr alloys are a new type of rare earth magnesium alloys, which are developed to address the problems facing the conventional magnesium alloys, such as poor elevated-temperature mechanical properties, low thermal stability and unsuitability for heat-treatment strengthening [1–4]. Recently, a series of Mg–Gd–Y–Zr alloys have been developed demonstrating that they can possess high strength, good creep resistance and strong precipitation-strengthening effect at elevated temperatures [5–7]. JANIK et al [5] strengthened a Mg–10Gd–3Y–0.4Zr alloy by peak-aging treatment, from which a high ultimate tensile strength above 300 MPa can be kept up to 250 °C. YU et al [6] fabricated a

high-strength Mg–11.7Gd–4.9Y–0.3Zr alloy using a combined technology of pre-deformation annealing, hot extrusion and aging, from which high yield strength of 500 MPa and moderate elongation of 2.7% were reached. The great achievements can considerably extend potential applications of Mg–Gd–Y–Zr alloys in elevated-temperature environments, even extending to the room and elevated-temperature tribological applications that used to be limited to aluminum alloys, such as sliding bearing, clutch piston and engine piston.

Up to now, a lot of researches have been devoted to tribological behavior of Mg alloys [8–13]. The most attractive investigation is the mild–severe (M–S) wear transition of Mg alloys. According to the result proposed by CHEN and ALPAS [14], Mg alloys exhibit two types of wear behavior, namely,

mild wear and severe wear. Mild wear proceeds in a steady state, in which wear rate increases gradually with augmentation of load or sliding velocity, and the surface is slightly damaged without severe plastic deformation (SPD) or massive material transfer to the counterface. Mild wear is thus acceptable in engineering applications, and it is usually regarded as a type of safe wear behavior. For this reason, discovery of mechanism of M–S wear transition and establishment of an effective criterion are two big issues in investigating wear characteristics of Mg alloys.

The M–S wear transition mechanism at room temperature has been explored under various loads and sliding velocities for several Mg alloys including AZ31, AZ51, AS31 and Mg97Zn1Y2 (at.%) alloys in previous studies [15–19]. It has been proven that the M–S wear transition mechanism is the softening of surface material as a result of the dynamic recrystallization (DRX) microstructure transformation during wear testing. This finding is essentially consistent with earlier wear experimental results of Mg and Al alloys [14,20]. Moreover, the most important factor governing the M–S wear transition of Mg alloys is a certain critical surface DRX temperature that depends on the sliding velocity [15,16,18].

Since only a limited number of research works have been carried out regarding tribological characteristics of Mg alloys at elevated temperatures [21–23], many tribological issues related with M–S wear transition need further understanding. ZAFARI et al [21] investigated the effect of load on wear rate of AZ91D alloy within 20–250 °C under a low sliding velocity of 0.4 m/s, and thought that the M–S wear transitions under different loads were decided at different critical contact surface temperatures. WANG et al [22] discovered that the critical load for M–S wear transition of AZ91D alloy reduced with rising test temperature during sliding at 0.5 ms⁻¹, and the existence of mechanically mixed layer (MML) on worn surface delayed M–S wear transition at 200 °C. Even though the available studies have identified the presence of mild wear and severe wear at elevated temperatures, the M–S wear transition mechanism for Mg alloys has not yet been fully clarified.

In this work, wear properties of Mg–10Gd–1.5Y–04Zr alloy were studied at temperatures of

20–200 °C. A high sliding velocity of 3.0 m/s was chosen for avoiding evident MML formation on worn surfaces and minimizing the influence of MML formation on the M–S wear transition. The mechanism for M–S wear transition was illustrated by the changes of microstructure and mechanical properties in subsurfaces. In addition, the relationship between normal load and critical temperature for M–S wear transition was also discussed on the basis of a critical surface DRX temperature criterion.

2 Experimental

2.1 Material

An ingot of Mg–Gd–Y–Zr alloy with 150 mm in diameter and 200 mm in length was prepared by the metal mold gravity casting process. The desired amounts of pure Mg, Mg–15%Gd, Mg–10%Y and Mg–5%Zr master alloys were heated to melt at 750 °C in a graphite crucible placed in a gas-protected electric furnace. After holding at 720 °C for 15 min, the melt was cast into a steel mold. The chemical composition of the ingot was examined by inductively coupled plasma emission spectrometry, as listed in Table 1. The prepared Mg–Gd–Y–Zr alloy is hereafter referred to as Mg–10Gd–1.5Y–04Zr alloy.

Table 1 Chemical composition of studied alloy (wt.%)

Gd	Y	Zr	Mg
10.1	1.5	0.4	Bal.

2.2 Wear testing

A MG–2000 type high-speed and high-temperature pin-on-disk wear tester was used for wear tests under unlubricated sliding condition. Pin specimens were machined from the casting ingot into dimensions of 6 mm in diameter and 13 mm in length. Disks were made of AISI 5150 steel by quenching and tempering to Rockwell hardness HRC57. Before commencement of wear testing, the surfaces of pins and disks were prepared by grinding with SiC papers and polishing to surface roughness of about 0.5 μm (R_a).

Wear tests were conducted within a temperature range of 20–200 °C under various loads of 10, 20, 30, 35, 40, 45, 50 and 60 N, respectively. For preventing MML from forming on the surfaces during wear testing, a high sliding

speed of 3.0 m/s was selected to wear out the oxide layer or MML as fully as possible. Each pin specimen was tested with a constant sliding distance, i.e. 565 m. The wear rate was expressed by the volumetric wear loss per unit sliding distance. The volumetric wear loss was calculated through the measured reduction of pin length before and after wear test using a micrometer with high measurement accuracy (± 0.0001 mm). Elevated-temperature wear tests were carried out in the split furnace. The required test temperatures were guaranteed to have an accuracy of ± 5 °C by using a chromel–alumel type thermocouple probe. At each test temperature, after holding temperature for about 15 min, wear testing started.

The morphologies of worn surfaces were analyzed by a TESCAN VEGA3 scanning electron microscope (SEM) equipped with an energy dispersive X-ray spectrometer (EDS). The microstructure change in subsurfaces of pins was examined after elevated-temperature wear tests using a LEXT-OLS3000 confocal scanning laser microscope. The microhardness distribution in subsurface was measured using a HVS–1000 microhardness tester with 100 g load for 15 s.

3 Results and discussion

3.1 Microstructure of Mg–10Gd–1.5Y–0.4Zr alloy

XRD analysis of Mg–10Gd–1.5Y–0.4Zr alloy identified the presence of α -Mg phase and Mg_5Gd phase, as shown in Fig. 1. The optical microscopy examination of the alloy showed that the metallographic structure consisted of equiaxed grains of α -Mg phase and discontinuous network of Mg_5Gd phase, as illustrated in Fig. 2. The average grain size of α -Mg phase was measured to be about 36 μm by linear intercept method. The Vickers hardness of the studied alloy was measured to be about HV 74.

In order to clarify the formation mechanism of the network of Mg_5Gd phase in the casting process, the thermal transformations in the studied alloy were examined in a continuous heating mode by differential thermal analysis (DTA), as shown in Fig. 3. The DTA thermal-gram exhibited two endothermic peaks at 444.5 and 628.1 °C, respectively. Their onset temperatures were 364.5 and 578.4 °C, respectively. By comparing the two

onset temperatures with those thermal transformation temperatures of Mg–10.1Gd alloy in Mg–Gd binary phase diagram, it was found that 364.5 °C was lower than the onset temperature for dissolution of Mg_5Gd precipitate phase, 389 °C, and 578.4 °C was also lower than the onset temperature for melting of α -Mg phase, 590 °C. The discrepancies between these temperatures could be due to the effect of other elements in the studied

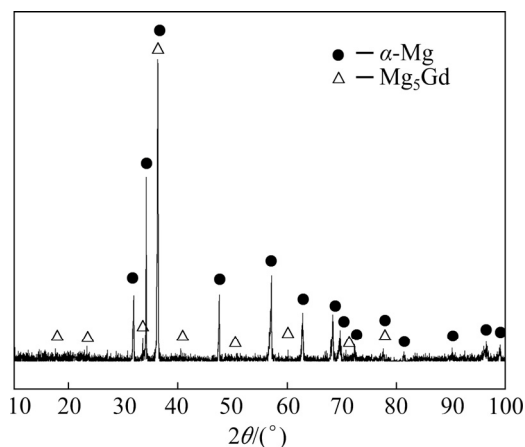


Fig. 1 XRD pattern of as-cast Mg–10Gd–1.5Y–0.4Zr alloy

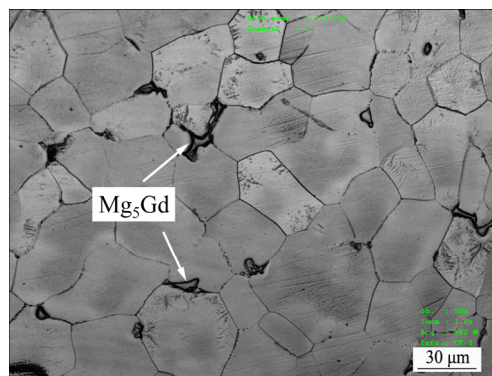


Fig. 2 Optical microstructure of studied alloy

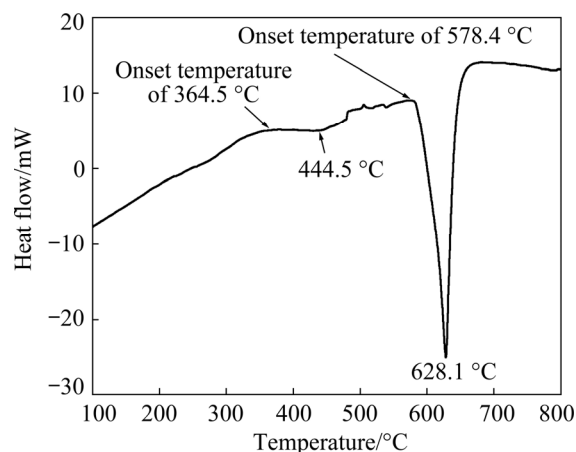


Fig. 3 DTA curve for studied alloy

alloy, such as Y and Zr. Since the maximum solubility of the element Gd in α -Mg solid solution phase is as high as 23.49% according to Mg–Gd binary phase diagram, the discontinuous network of Mg₅Gd phase can be confirmed to originate from precipitation rather than eutectic reaction during the cooling process.

3.2 Effect of load and test temperature on wear rate

Wear rate–test temperature curves under various loads are shown in Fig. 4. The curves were divided into three groups with regarding to the variation trend with test temperature. The first group only included the curve under normal load of 10 N. Its wear rate increased fast in the temperature range of 20–50 °C, then maintained a low value below $18 \times 10^{-12} \text{ m}^3/\text{m}$ throughout the temperature range of 50–200 °C. The second group consisted of the curves under the loads of 20, 30, 35, 40 and 45 N. Their wear rates also increased fast within 20–50 °C, then maintained low levels within different certain temperature ranges, and finally rose rapidly with further increasing temperature. The corresponding temperature ranges for rapid increasing and maintaining of wear rate were 20–185, 20–135, 20–100, 20–75 and 20–50 °C when normal loads were 20, 30, 35, 40 and 45 N, respectively. It is noticeable that the maintaining temperature range decreases with increasing load, i.e. decreasing from a width of 50–185 °C under 20 N to a single point, 50 °C, under 45 N. The test temperatures at the turning points could be consequently confirmed as 185 °C under 20 N, 135 °C under 30 N, 100 °C under 35 N, 75 °C under 40 N and 50 °C under 45 N, respectively. The wear rates at the turning points were all smaller than $17 \times 10^{-12} \text{ m}^3/\text{m}$. Furthermore, it was also found that they were very close to the wear rates of AZ51 and AS31 alloys under their respective M–S wear transition loads, namely $12.5 \times 10^{-12} \text{ m}^3/\text{m}$ under 50 N for AZ51 alloy and $13.5 \times 10^{-12} \text{ m}^3/\text{m}$ under 60 N for AS31 alloy [16,18]. Therefore, it is reasonable to deduce that the turning points on wear rate–test temperature curves actually correspond to the M–S wear transitions according to the definition given by CHEN and ALPAS [14].

The third group was composed of the curves under 50 and 60 N. Both wear rates went up rapidly in a large slope within 20–100 °C, then suddenly

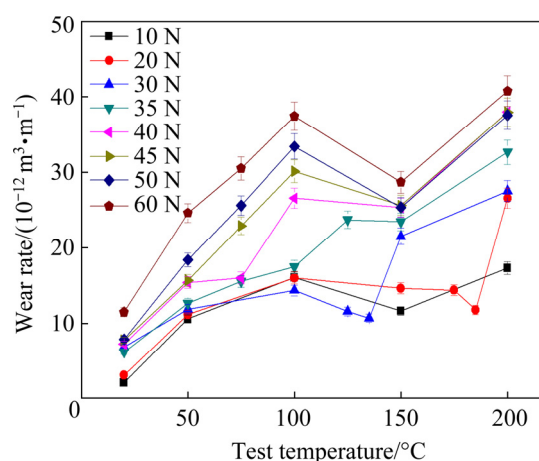


Fig.4 Variations of wear rates with test temperature under various applied loads

dropped at 150 °C, and finally rose again at 200 °C. Even though the two wear rate curves appear to have a variation trend similar to that under 45 N, the wear rates at 50 °C were much larger under 50 and 60 N than under 45 N. They are actually in the severe wear regime. Therefore, the wear-rate curve under 45 N was not included in the third group. In addition, it was also noticed that the wear rate more or less dropped when test temperature was higher than 100 °C, especially an evident dropping occurred at 150 °C under the loads of 40–60 N. This phenomenon could be related with a certain type of strengthening mechanism operating in the studied alloy when test temperature was higher than 100 °C.

3.3 Wear mechanisms

The morphologies and chemical compositions of worn surfaces were analyzed using SEM and EDS techniques. The contents of major elements on the worn surfaces are listed in Table 2. SEM micrographs of worn surfaces are shown in Fig. 5. The surfaces worn at 20 °C in mild wear displayed typical delamination scars and small detached pieces of oxide layer, just like the morphological features of worn surface at 20 N and 20 °C (Fig. 5(a)). Meanwhile, the contents of oxygen element were quite high on the worn surfaces, for example, 13.04% at 20 N and 7.99% at 40 N. The corresponding wear mechanisms were delamination and surface oxidation (SO). However, it was found that these surface morphological features appeared not evident at elevated temperatures, i.e. the number of delamination scar decreased and the surfaces

Table 2 Contents of major elements on worn surfaces

Load/N	Temperature/°C	Content/wt.%			
		O	Gd	Y	Zr
10	50	3.85	9.08	1.62	0.55
	100	7.68	9.23	1.53	0.39
	150	3.86	9.28	1.62	0.51
	200	3.05	9.19	1.41	0.63
30	50	3.10	9.18	1.68	0.53
	100	1.92	9.17	1.50	0.56
	150	5.16	8.80	1.30	0.50
	200	3.72	8.67	1.50	0.75
40	20	7.99	8.90	1.28	0.44
	50	1.76	9.29	1.71	0.54
	75	2.49	9.60	1.40	0.35
	150	3.98	9.29	1.46	0.30
	200	1.58	8.94	1.49	0.54
60	20	3.80	9.61	1.39	0.35
	50	3.85	9.06	1.48	0.55
	100	5.82	9.04	1.43	0.47
	150	1.78	9.10	1.44	0.44
	200	1.17	9.33	1.55	0.62

became flat. Moreover, a few of wear mechanisms that usually occurred at room temperature in mild wear regime for magnesium alloys, such as oxidation, abrasion and delamination, disappeared at elevated temperatures above 50 °C. For the first group of wear rate curve, i.e. under 10 N, the worn surfaces at 50 and 100 °C were suffered from mild plastic deformation (MPD) and a few spallation scars of oxide layer, which resulted in a flatten surface and a few shallow detachment scars of oxide layer (Fig. 5(b)). The contents of oxygen element were 3.85% and 7.68%, respectively. As seen from the top right photograph showing the edge of the specimen, the surface material was plastically deformed along the sliding direction, but was not extruded out the contact surface. These features indicate that MPD and SO are the major wear mechanisms. As test temperature was increased above 100 °C, the surface was characterized by a smooth appearance along with a few of scratches and scars (Fig. 5(c)), meanwhile the surface material was still restricted between the contact surfaces. The contents of oxygen element were 3.86% at 150 °C and 3.05% at 200 °C,

respectively. Therefore, the primary wear mechanisms were MPD, scratch and slight surface oxidation. It is noted that even in the mild wear regime, the content of oxygen element do not invariably increase with increasing test temperature. This could be related with the enhancement of MPD at high temperature, because the brittle oxide film or layer was easily broken and removed from the deformed surface at high sliding speed.

For the second group of wear rate curves, for example, when subjected to 40 N, the worn surfaces were also slightly deformed at 50 and 75 °C (Figs. 5(d) and (e)). Even though the worn surface was much even at 75 °C, the surface material was still limited between the contact surfaces and a few cracks were found on localized area. The oxygen element content declined to a very low extent, only 1.76%–2.49%. The main mechanism was thus MPD. However, at temperatures above 75 °C, surface material underwent SPD and was extruded out the contact surface, resulting in a rather smooth surface and a bending edge (Fig. 5(f)). In addition, there were no scars and cracks on the surface, indicating that the surface material exhibits a better ductility at temperatures above 75 °C. This suggests that wear mechanism transforms from MPD to SPD.

For the third group of wear rate curves, when a high load of 60 N was applied, the worn surface demonstrated typical SPD features even at 20 °C, that is, the worn surface was very smooth without cracks, and the extruded surface material produced a bending edge (Fig. 5(g)). The bending edge was much more obvious as test temperature was increased to 50 °C (Fig. 5(h)). This could be due to the thermal softening originating from frictional heating produced by large load and high sliding velocity.

As for the dropping of wear rates at temperatures above 100 °C, the surface oxidation was found not to be the dominant cause, since the content of oxygen element was rather low at 150 °C under the loads of 40–60 N, ranging from 1.78% to 3.98%. Such a low content of oxygen element was insufficient to produce a hard oxide layers that could cover the entire worn surface and decrease wear rate considerably. From the aspect of casting process of the studied alloy, the precipitation hardening that occurred during wear testing at elevated temperatures might be a major reason for

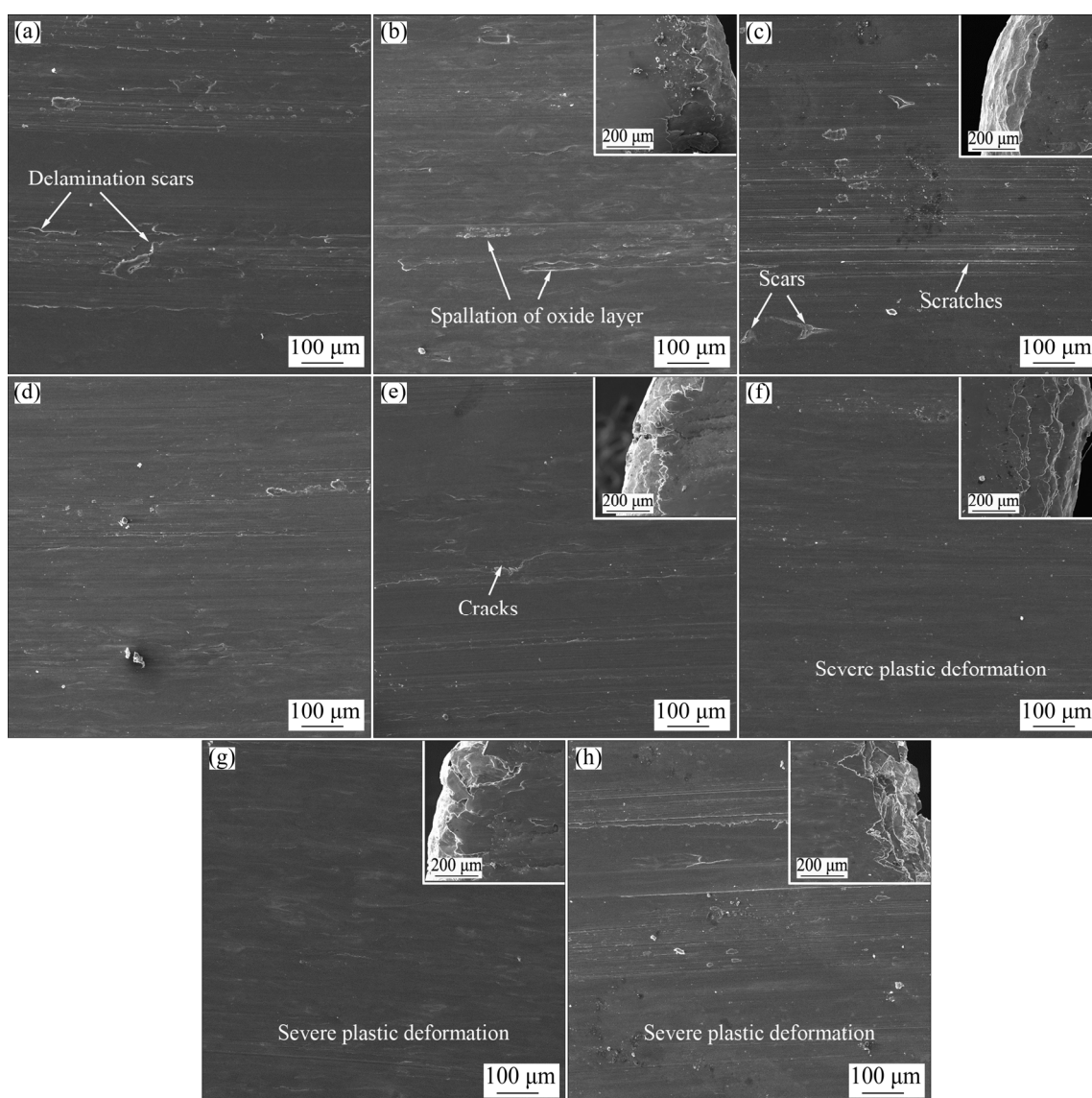


Fig. 5 SEM images of worn surfaces under different sliding conditions: (a) 20 N, 20 °C; (b) 10 N, 50 °C; (c) 10 N, 200 °C; (d) 40 N, 50 °C; (e) 40 N, 75 °C; (f) 40 N, 150 °C; (g) 60 N, 20 °C; (h) 60 N, 50 °C

the dropping of wear rate. In fact, the α -Mg phase was in a super-saturated state owing to fast cooling velocity during steel mold casting, and precipitation could happen at test temperatures above 100 °C. SMOLA et al [24] reported that intermetallic phases precipitated in as-cast Mg–Gd–Y–Zr alloys such as Mg–10Gd, Mg–15Gd and Mg–10Gd–3Y–0.5Zr alloys during heating at temperatures ranging from 100 to 250 °C, in which phase transformation developed in the following sequence: supersaturated solid solution α' (hcp) \rightarrow β'' (D019) \rightarrow β' (cbco) \rightarrow β (Mg₅Gd, fcc).

In order to testify the deduction of precipitation hardening, cylindrical samples of 8.0 mm in diameter and 10.0 mm in length were

directly machined from the studied alloy for aging test. The samples were heat-treated in an electron resistance furnace without protection of shield gas at temperatures of 50–200 °C during a period of 20 min (almost the same period of wear testing). After standard surface preparation including grinding with SiC sand paper and polishing with diamond paste, the hardness was measured using a HVS–1000 microhardness tester. The average hardness values after aging at different temperatures are listed in Table 3. The hardness measurement results identified the precipitation hardening phenomenon at temperatures of 150–200 °C. The hardness was enhanced significantly above 100 °C, i.e., increased from HV 74.1 at 20 °C to HV 81.5 at

150 °C. In fact, several Mg–Gd–Y–Zr alloys have been reported to exhibit significant strengthening effect after aging at temperatures of 180–200 °C for a short period. NING et al [25] reported that hot-rolled Mg–10Gd–3Y–2Ag–0.4Zr alloy exhibited a hardness increase from HV 95 to HV 113 after aging at 180 °C for 24 min.

Table 3 Hardness results of as-cast alloy after aging at different temperatures

Temperature/°C	Hardness (HV)
20	74.1
50	75.6
100	78.5
150	81.5
200	82.3

A wear mechanism transition map of the studied alloy was established on test temperature–normal load coordinate system, as shown in Fig. 6. It consisted of two major regions, namely mild and severe wear regions. The boundary between them was indicated by solid line AA' . Each region was composed of several sub-regions. The mild wear region (considered as safe working region) included three main sub-regions. They were delamination+surface oxidation, MPD+surface oxidation and MPD+scratch sub-regions, respectively. At the temperatures of 50–200 °C, the surface oxidation mainly occurred as the normal load was not higher than 10 N. Here, we defined the surface oxidation as the content of oxygen element on the worn

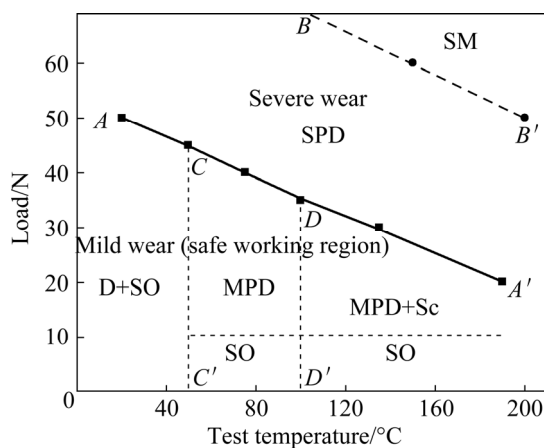


Fig. 6 Wear mechanism transition map (D–Delamination; MPD–Mild plastic deformation; SO–Surface oxidation; SPD–Severely plastic deformation; SM–Surface melting; Sc–Scratch)

surface was larger than 3.0%. The severe wear region was composed of two sub-regions, i.e., SPD and surface melting (SM) sub-regions that were separated by dashed line BB' . The boundary lines CC' and DD' were determined by the absence of delamination wear mechanism and occurrence of scratching, respectively.

3.4 M–S wear transition mechanism

As observed from the wear mechanism transition map, a common point was noted that the onset of M–S wear transitions was accompanied by the wear mechanism transition from MPD to SPD under loads of 20–45 N. This phenomenon suggests that the occurrence of SPD is possibly related with a certain type of microstructure transformation in surface material and the consequent property change. The microstructure and microhardness in subsurfaces were therefore examined for several selected pin specimens tested under 30, 40 and 60 N in mild and severe wear regimes, as shown in Figs. 7 and 8, respectively.

Under the load of 30 N, at 50 °C, a deformed microstructure zone with a thickness of about 170 μm was formed in the subsurface (Fig. 7(a)). As seen in the magnification photograph (Fig. 7(b)), a considerable amount of deformation twins were produced in α -Mg grains along the deformation direction. At 100 °C, the deformed microstructure zone was extended to about 180 μm in depth (Fig. 7(c)). However, when test temperature was further increased to 150 °C, besides formation of a friction-affected zone (FAZ) with a depth of 190 μm , another important finding was that a quite different microstructure of the original deformed microstructure in the top part of FAZ took place, namely a newly formed microstructure consisting of fine grains in submicrometer scale was developed within 0–50 μm in depth (Fig. 7(d)). These fine grains might be formed by DRX transformation, since the combination of large plastic strain and high surface temperature rising in the near-surface region enable DRX transformation to realize. With the test temperature reaching the highest temperature of 200 °C, the microstructure transformation in subsurface became more complicated. It is known from metallic recrystallization theory that the plastically deformed magnesium alloys undergo static recrystallization (SRX) when heating temperature is higher than

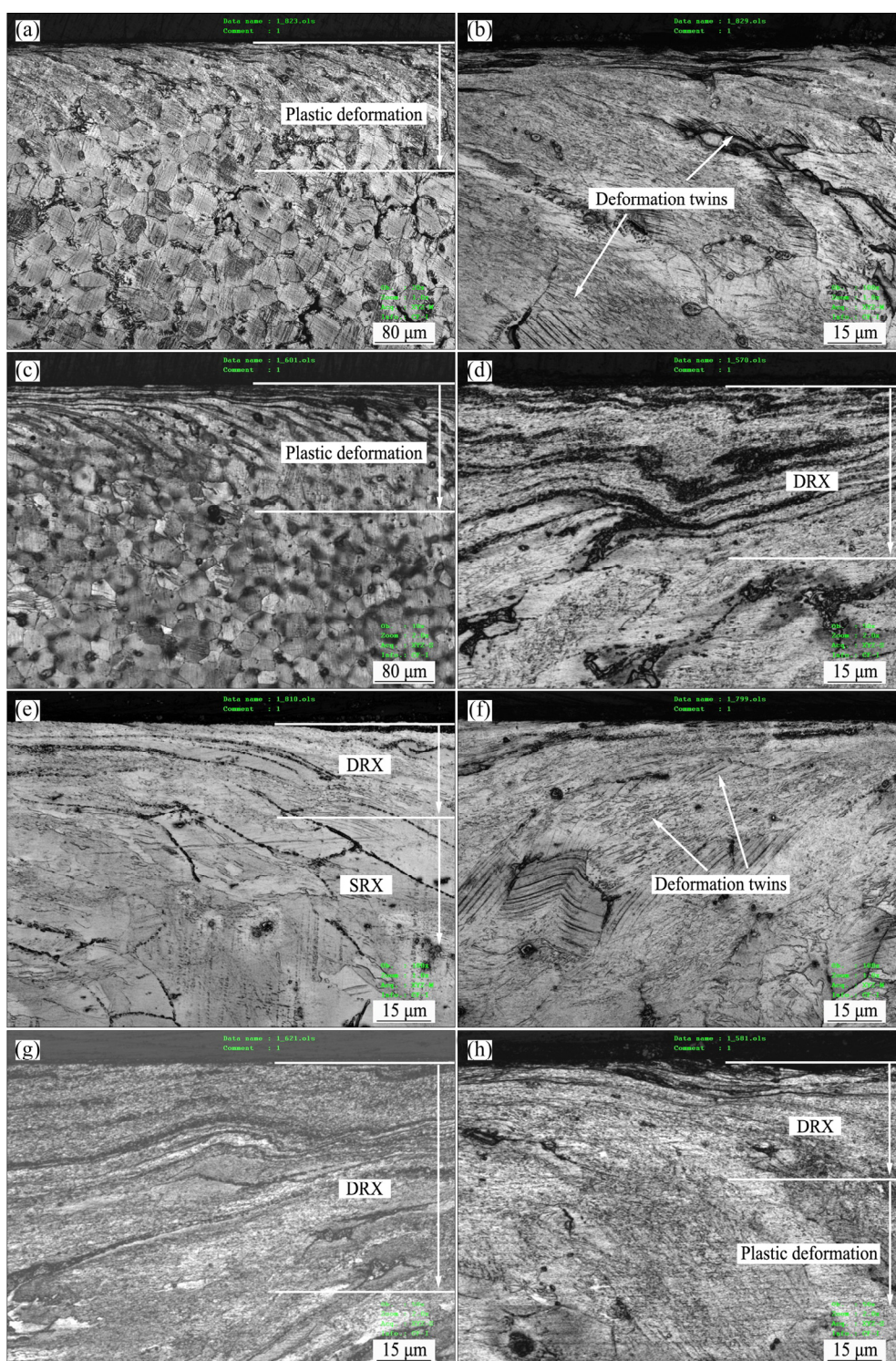


Fig. 7 Microstructures in subsurfaces under different conditions: (a, b) 30 N, 50 °C; (c) 30 N, 100 °C; (d) 30 N, 150 °C; (e) 30 N, 200 °C; (f) 40 N, 50 °C; (g) 40 N, 100 °C; (h) 60 N, 20 °C

150 °C. Therefore, at 200 °C, below the top DRX microstructure zone was actually a zone of SRX microstructure along with deformed α -Mg grains within the depth of 30–100 μm (Fig. 7(e)). In contrast to the continuous dynamic deformation in near surface zone, an almost static deformation

zone with a steady-state plastic strain distribution was formed below. Such a distribution of steady-state plastic strain in the subsurfaces was found in several magnesium alloys even after a short period of sliding wear [26]. This type of strain distribution can promote SRX microstructure transformation

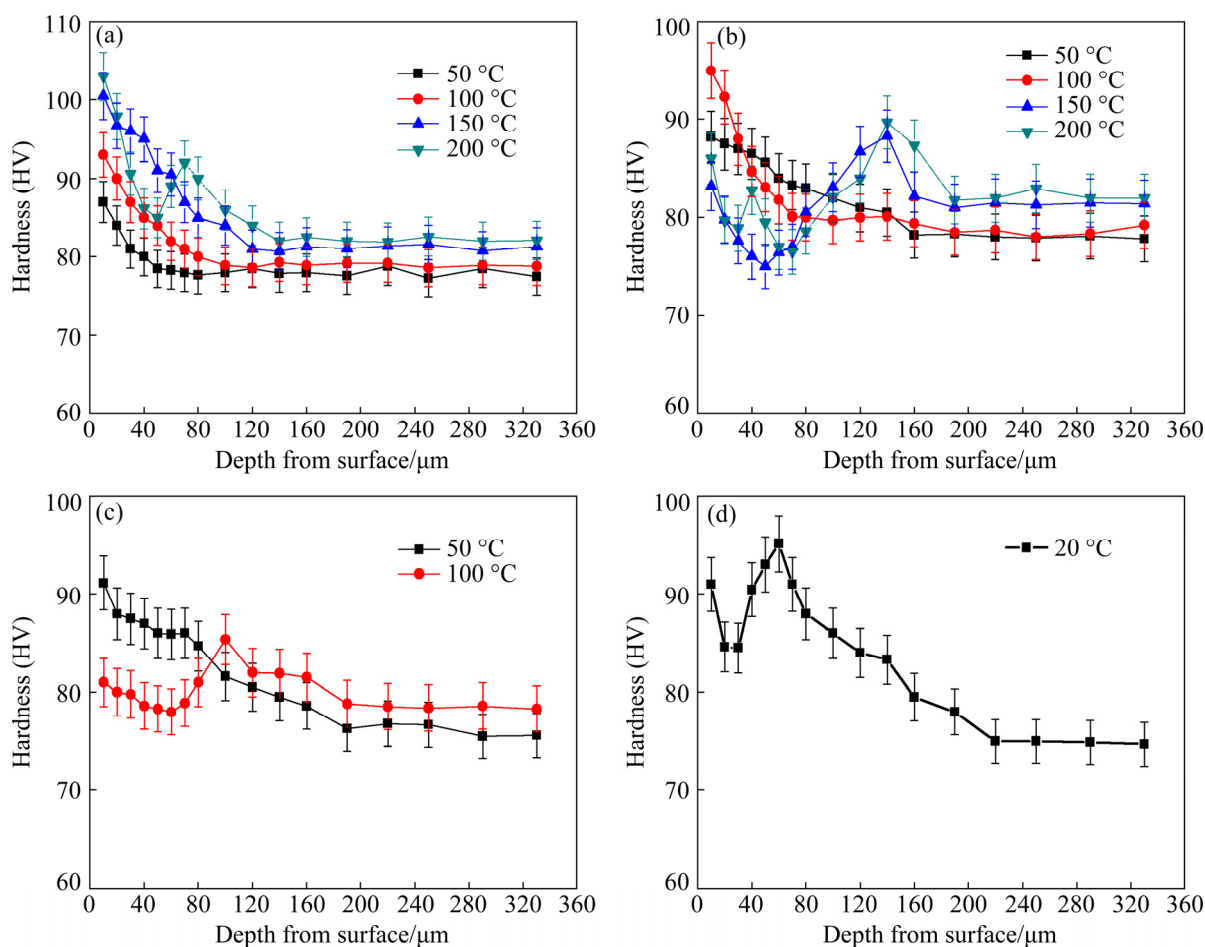


Fig. 8 Microhardness vs depth from surface under different loads: (a) 10 N; (b) 30 N; (c) 40 N; (d) 60 N

within a certain depth range in subsurface as long as the test temperature is higher than 150 °C. Under 40 N, a similar transformation from plastic deformation to DRX microstructure was found in the near surface region before and after the critical temperature of 75 °C ((Figs. 7(f) and (g)). Under the highest load of 60 N, DRX microstructure transformation was found to be realized within the 0–30 μm depth even at 20 °C (Fig. 7(h)).

Since DRX softening typically accompanies the DRX microstructure transformation, the microhardness in the subsurface was measured to verify the softening effect, as shown in Fig. 8. Under the lowest load of 10 N, the hardness increased within 20 μm depth with temperature rising, even through a rapid decrease of hardness occurred at depth above 20 μm as temperature was 200 °C (Fig. 8(a)). This means that there is no softening in the near-surface region in the mild wear regime. However, the softening of surface material was observed in specimens suffered from

severe wear. Under the load of 30 N, when wear was mild at 50 and 100 °C, the hardness reduced monotonically along the depth direction until the hardness of unaffected substrate, suggesting strain-hardening effect decreasing with the increase in depth (Fig. 8(b)). The hardness was found to be higher at 100 °C than at 50 °C within 30 μm in depth. This could be due to the combination of an enhanced strain-hardening effect by larger plastic deformation extent and an evident precipitation hardening effect at 100 °C. When wear was severe at 150 and 200 °C, the hardness values were much lower than those at 50 and 100 °C within 80 μm in depth, suggesting the occurrence of softening. The hardness curve exhibited a V-shaped valley at 50 °C, but a W-shaped variation at 100 °C within the softening depth range. In comparison with subsurface microstructures in Figs. 7(d) and (e), the V-shaped valley at 50 °C actually corresponded to DRX microstructure transformation zone, while W-shaped variation range corresponded to DRX

and SRX microstructure transformation zones. Under 40 N, at 100 °C, a low hardness valley was also formed within 70 μm in depth, whereas at 50 °C, the hardness decreased monotonically throughout the entire plastic deformation zone (Fig. 8(c)). The low valley of hardness apparently corresponded to the DRX microstructure zone. Similarly, under 60 N, a low hardness valley also occurred within 30 μm in depth even at 20 °C (Fig. 8(d)). The difference between the hardness distributions in subsurfaces prior to and after M–S wear transition confirms that DRX softening in the near surface region is the real cause of M–S wear transition.

3.5 Relation of normal load with test temperature for M–S wear transition

The M–S wear transition mechanism of magnesium alloys during dry sliding wear at room temperature has been proven to be the softening of surface layer material owing to DRX microstructure transformation by several research works [15–19]. LIANG et al [15–17] and AN et al [18,19] have proposed a surface DRX temperature criterion of M–S wear transition for magnesium alloys on the basis of comprehensive studies of AZ31, Mg–5Al–0.8Zn, Mg–3Al–0.4Si–0.1Zn and Mg97Zn1Y2 alloys. The surface DRX temperature criterion tells that when friction-induced surface temperature (T_s) exceeds a critical DRX temperature (T_{DRX}), i.e. $T_s \geq T_{DRX}$, mild wear transits into severe wear. The critical DRX temperature only depends on the sliding speed. A model for evaluating the transition load (F_T) is established according to the surface DRX temperature criterion of M–S wear transition, as expressed by Eqs. (1) and (2). These two equations are actually derived from the relation of friction-induced surface temperature (T_b) with normal load (F) and sliding velocity (v) proposed by LIM and ASHBY [27], as expressed by Eq. (3).

$$F_T = \frac{(T_{DRX} - T)}{c_{DRX} \mu v} \quad (1)$$

$$c_{DRX} = \frac{\alpha l_b}{A_n K_{mp}} \quad (2)$$

$$T_b = T + \frac{\alpha \mu F v l_b}{A_n K_{mp}} \quad (3)$$

where T is the environmental temperature, c_{DRX} is

an approximate constant that is related to the material properties of friction pair, μ is the coefficient of friction, and A_n , l_b , K_{mp} and α stand for the nominal contact area, mean diffusion distance, thermal conductivity and conducted heat fraction of the pin, respectively.

In the present study, it is noted that at M–S wear transition state, normal load shows a perfect linear relation with test temperature within 20–190 °C, i.e. raising test temperature decreases the required normal load, as shown by solid line AA' in Fig. 6. After linearly fitting as shown in Fig. 9, the normal load can be written as a linear function of test temperature T , i.e. Eq. (4), and it can also be expressed by Eq. (5).

$$F_T = kT + F_0 \quad (4)$$

$$F_T = -k(T_0 - T) \quad (5)$$

where F_0 and T_0 are the intercepts of F_T and T axes, respectively, their respective values are 53.4 N and 302.9 °C, and k is the slope of linear relationship, -0.1764 . The physical meaning of F_0 is the transition load when test temperature is 0 °C, as shown from the fitted line. Nevertheless, the meanings of k and T_0 cannot be easily determined from the fitted line. However, it is found that Eq. (5) is similar to Eq. (1), i.e., the modeling of M–S wear transition load for Mg alloys at room temperature was put forth by LIANG et al [15,16]. If the surface DRX temperature criterion can be applied to dry sliding wear at elevated temperatures, transition load should have a linear relationship with test temperature under a constant sliding speed, given that c_{DRX} and μ are not evidently influenced by test temperature, i.e., they can be roughly regarded as

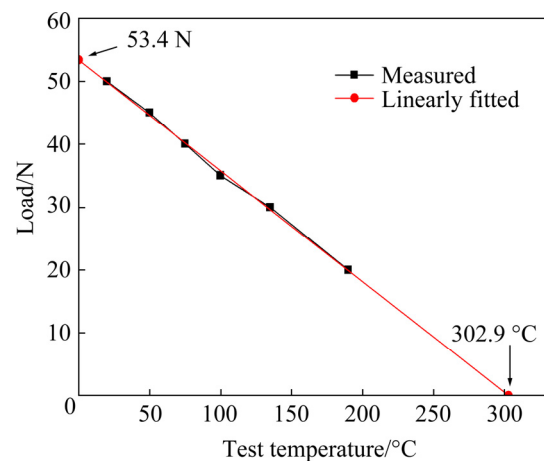


Fig. 9 Curves of normal load vs test temperature for M–S wear transition

constants. Therefore, as seen from the linear relationship between F_T and T , the Mg–10Gd–1.4Y–0.4Zr alloy could follow the surface DRX temperature criterion during the dry sliding wear at temperatures of 50–200 °C.

By comparison of Eq. (1) with Eq. (5), it can be seen that T_0 and $-k$ correspond to T_{DRX} and the reciprocal of $c_{DRX}\mu v$, respectively. In the present study, the coefficient of friction μ varied narrowly around 0.32 at different M–S wear transition states, and sliding velocity was a constant of 3.0 m/s. c_{DRX} is therefore calculated to be 5.905 using the values of k , μ and v . At the different M–S wear transition states, l_b , A_n and α could be considered as nearly constants since the reduction in length of pins was very small compared with their original length. As for the thermal conductivity of pin (K_{mp}), it is reported that thermal conductivity increases a little at 50–200 °C for magnesium alloys. For instance, thermal conductivity varies from 105 to 107 W/(m·K) for Mg–1.5%Al alloy, from 137 to 142 W/(m·K) for Mg–1.0%Zn alloy, from 57 to 64 W/(m·K) for Mg₉₇Zn₁Y₂ alloy, from 51 to 57 for aged Mg₉₇Zn₁Gd₂ alloy [28–31]. The almost constant μ at the different M–S wear transition states could be due to the same surface DRX temperature and similar surface morphologies even though the test temperatures were different. Therefore, for the reason of simplification, c_{DRX} can be approximately taken as a constant at different M–S wear transition states. In order to confirm if T_0 302.9 °C was the critical DRX temperature of surface material under given sliding velocity condition, the strain rate of surface material plastic deformation was measured after wear testing, and then hot compression tests were conducted at a similar strain rate within a temperature range of 250–350 °C.

The equivalent shear strain was measured by means of the curvature of the flow line under two siding conditions in mild wear, and then was plotted against depth from the surface, as shown in Fig. 10. The equivalent strain $\varepsilon(z)$ at the depth z was calculated using the shear angle of the flow line $\theta(z)$, as expressed by Eq. (6) [32,33].

$$\varepsilon(z) = \frac{\sqrt{3}}{3} \tan \theta(z) \quad (6)$$

The equivalent strain was very large near the

surface. The strain was higher than 1.0 within 5–40 μm in depth under 30 N and 100 °C, and within the 5–80 μm depth under 40 N and 50 °C, respectively. The corresponding strain rate varied from 5.3×10^{-3} to $3.5 \times 10^{-2} \text{ s}^{-1}$ within 5–40 μm in depth under 30 N and 100 °C, and from 5.3×10^{-3} to $5.6 \times 10^{-2} \text{ s}^{-1}$ within 5–80 μm in depth under 40 N and 50 °C. Since friction-induced DRX microstructure transformation occurred in the two depth ranges under 30 and 40 N, the strain rates in the middle of the two depth ranges could be approximately took as $1.0 \times 10^{-2} \text{ s}^{-1}$. Therefore, hot compression tests were performed with strain rate of $1.0 \times 10^{-2} \text{ s}^{-1}$ until true strain of 1.0 in the temperature range of 250–350 °C for determination of DRX temperature.

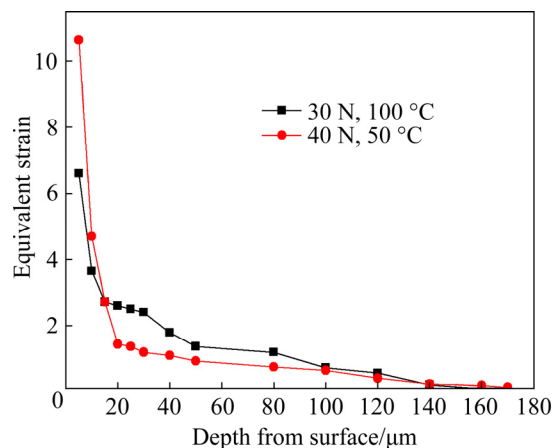


Fig. 10 Curves of equivalent plastic strain vs depth from surface

After hot compression testing, the optical microstructures of the samples were examined. The microstructures of hot compressed samples at 290 and 300 °C are shown in Fig. 11. At 290 °C, a series of deformation twins were formed in α -Mg grains, while at 300 °C, a lot of fine DRX grains occurred. The DRX grains evidently grew at the original locations of twins. The critical temperature for DRX microstructure transformation at $1.0 \times 10^{-2} \text{ s}^{-1}$ was consequently considered as 300 °C. The DRX temperature determined in hot-compression tests essentially agrees with the linearly fitted T_0 , 302.9 °C. Therefore, it is reasonable to conclude that the M–S wear transition of Mg–10Gd–1.5Y–0.4Zr alloy at elevated test temperature still follows the critical temperature criterion by LIANG et al [15,16].

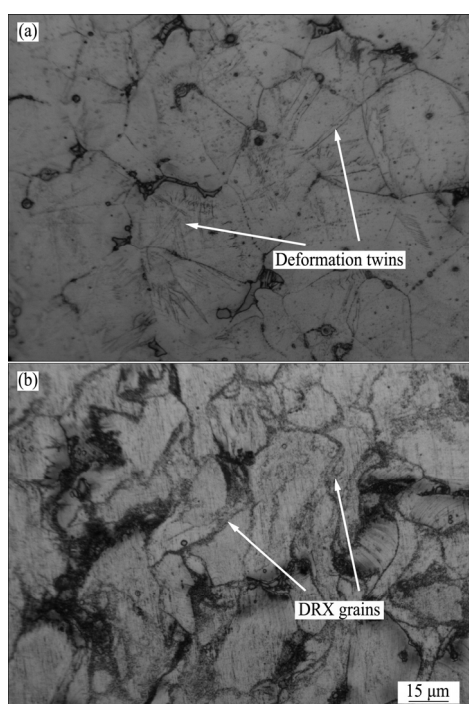


Fig. 11 Microstructures after hot compression at different temperatures: (a) 290 °C; (b) 300 °C

4 Conclusions

(1) There were evident turning points on the wear rate vs test temperature curves under normal loads of 20–45 N. The wear rate increased rapidly as test temperature exceeded the critical value at turning point. The turning points actually corresponded to the M–S wear transitions.

(2) The critical temperature for M–S wear transition decreased from 185 to 20 °C with increasing normal load from 50 to 20 N.

(3) In mild wear region, the main wear mechanisms were delamination, surface oxidation, MPD and scratch. In severe wear region, the major wear mechanisms were SPD and surface melting.

(4) In mild wear, surface material underwent plastic deformation and consequently was strain-hardened, while in severe wear, surface material experienced DRX microstructure transformation and therefore was softened.

(5) The normal load presents an almost linear relationship with the critical temperature for M–S wear transition. The good agreement between the linearly fitted DRX temperature and hot-compression result proves that M–S wear transition at elevated temperatures obeys the surface DRX temperature criterion.

Acknowledgments

The authors are grateful for the financial support from the National Natural Science Foundation of China (No. 51775226)

References

- [1] LI J L, WU D, CHEN R S, HAN E H. Anomalous effects of strain rate on the room-temperature ductility of a cast Mg–Gd–Y–Zr alloy [J]. *Acta Materialia*, 2018, 159: 31–45.
- [2] ZHANG F, WANG Y F, DUAN Y B, WANG K J, WANG Y T, ZHANG W J, HU J. Precipitation process during the peak-aged and over-aged stages in an Mg–Gd–Y–Zr alloy [J]. *Journal of Alloys and Compounds*, 2019, 788: 541–548.
- [3] WANG Q, MU Y, LIN J, ZHANG L, ROVEN H J. Strengthening and toughening mechanisms of an ultrafine grained Mg–Gd–Y–Zr alloy processed by cyclic extrusion and compression [J]. *Materials Science and Engineering A*, 2017, 699: 26–30.
- [4] DING Zhi-bing, ZHAO Yu-hong, LU Ruo-peng, YUAN Mei-ni, WANG Zhi-jun, LI Hui-jun, HOU Hua. Effect of Zn addition on microstructure and mechanical properties of cast Mg–Gd–Y–Zr alloys [J]. *Transactions of Nonferrous Metals Society of China*, 2019, 29(4): 722–734.
- [5] JANIK V, YIN D D, WANG Q D, HE S M, CHEN C J, CHEN Z, BOEHLERT C J. The elevated-temperature mechanical behavior of peak-aged Mg–10Gd–3Y–0.4Zr alloy [J]. *Materials Science and Engineering A*, 2011, 526: 3105–3112.
- [6] YU Z, XU C, MENG J, KAMADO S. Microstructure evolution and mechanical properties of a high strength Mg–11.7Gd–4.9Y–0.3Zr (wt%) alloy prepared by pre-deformation annealing hot extrusion and ageing [J]. *Materials Science and Engineering A*, 2017, 703: 348–358.
- [7] ZHENG L, LIU C, WAN Y, YANG P, SHU X. Microstructure and mechanical properties of Mg–10Gd–6Y–2Zn–0.6Zr (wt.%) alloy [J]. *Journal of Alloys and Compounds*, 2011, 509: 8832–8839.
- [8] AN J, LI R G, LU Y, CHEN C M, XU Y, CHEN X, WANG L M. Dry sliding wear behavior of magnesium alloys [J]. *Wear*, 2008, 265: 97–104.
- [9] EI-MORSY A W. Dry sliding wear behavior of hot deformed magnesium AZ61 alloy as influenced by the sliding conditions [J]. *Materials Science and Engineering A*, 2008, 473: 330–335.
- [10] TALTAVULL C, TORRES B, LOPEZ A J, RAMS J. Dry sliding wear behavior of AM60B magnesium alloy [J]. *Wear*, 2013, 301: 615–625.
- [11] SELVAN S A, RAMANATHAN S. A comparative study of the wear behavior of as-cast and hot extruded ZE41A magnesium alloy [J]. *Journal of Alloys and Compounds*, 2010, 502: 495–502.
- [12] KUMAR S, KUMAR D, JAIN J, HIRWANI J K. Influence of load, sliding speed and microstructure on wear response of AZ91 Mg alloy [J]. *Proceedings of the Institution of Mechanical Engineering. Part J: Journal of Engineering Tribology*, 2016, 230: 1462–1469.

- [13] HU Mao-liang, WANG Qu-dong, JI Ze-sheng, XU Hong-yu, XIN Ming-de, MA Guo-rui. Wear behavior of Mg–10Y–4Gd–1.5Zn–0.4Zr alloy [J]. Transactions of Nonferrous Metals Society of China, 2016, 26(12): 406–413.
- [14] CHEN H, ALPAS A T. Sliding wear map for the magnesium alloy Mg–9Al–0.9Zn (AZ91) [J]. Wear, 2000, 246: 106–116.
- [15] LIANG C, LI C, L X X, AN J. Correlation between friction-induced microstructural evolution, strain hardening in subsurface and tribological properties of AZ31 magnesium alloy [J]. Wear, 2014, 312: 29–39.
- [16] LIANG C, SU T F, WANG Y B, HAN X, YIN M L, AN J. An investigation on transition between mild and severe wear in Mg–5Al–0.8Zn magnesium alloy using recrystallization kinetics modeling [J]. Journal of Tribology—Transactions of the ASME, 2015, 137: 031602.
- [17] LIANG C, HAN X, SU T F, LI C, AN J. Sliding map for AZ31 magnesium alloy [J]. Tribology Transactions, 2014, 57: 1077–1085.
- [18] AN J, SUN W, NIU X D. Dry sliding wear behavior and a proposed criterion for mild to severe wear transition of Mg–3Al–0.4Si–0.1Zn alloy [J]. Tribology Letters, 2017, 65: 98.
- [19] AN J, XUAN X H, ZHAO J, SUN W, LIANG C. Dry sliding wear behavior and subsurface microstructure evolution of Mg97Zn1Y2 alloy in a wide sliding speed range [J]. Journal of Materials Engineering and Performance, 2017, 26: 4940–4952.
- [20] ZHANG J, ALPAS A T. Transition between mild and severe wear in aluminum alloys [J]. Acta Materialia, 1997, 45: 513–518.
- [21] ZAFARI A, GHASEMI H M, MAHMUDI R. Tribological behavior of AZ91D magnesium alloy at elevated temperatures [J]. Wear, 2012, 292–293: 33–40.
- [22] WANG S Q, YANG Z R, ZHAO Y T, WEI M X. Sliding wear characteristics of AZ91D alloy at ambient temperatures of 25–200 °C [J]. Tribology Letters, 2010, 38: 39–45.
- [23] LABIB F, GHASMI H M, MAHMUDI R. Dry tribological behavior of Mg/SiC_p composites at room and elevated temperatures [J]. Wear, 2016, 348–349: 69–79.
- [24] SMOLA B, STULIKAVA I, BUCH VON F, MORDIKE B L. Structural aspects of high performance Mg alloys [J]. Materials Science and Engineering A, 2002, 324: 113–117.
- [25] NING H Y, YU Y D, GAO B, XIAO L R, WEN L H, YAN Z H, LI L, CHEN X F. Grain refinement and aging hardening of the Mg–10Gd–3Y–2Ag–0.4Zr alloy produced by a two-step forming process [J]. Materials, 2018, 11: 757.
- [26] DAS S, MORALES A T, ALPAS A T. Microstructural evolution during high temperature sliding wear of Mg–3%Al–1%Zn (AZ31) alloy [J]. Wear, 2010, 268: 94–103.
- [27] LIM S C, ASHBY M F. Wear-mechanism maps [J]. Acta Metallurgica, 1987, 35: 1–24.
- [28] YING T, ZHENG M Y, LI Z T, QIAO X G. Thermal conductivity of as-cast and as-extruded binary Mg–Al alloys [J]. Journal of Alloys and Compounds, 2014, 608: 19–24.
- [29] YING T, ZHENG M Y, LI Z T, QIAO X G, XU S W. Thermal conductivity of as-cast and as-extruded binary Mg–Zn alloys [J]. Journal of Alloys and Compounds, 2015, 621: 250–255.
- [30] TROJANOVA Z, HALMESOVA K, DROZD Z, SIMA V, LUCAC P, DZUGAN J, MINARIK P. Thermal conductivity of an AZ31 sheet after accumulative roll bonding [J]. Crystals, 2018, 8: 278.
- [31] YAMASAKI M, KAWAMURA Y. Thermal diffusivity and thermal conductivity of Mg–Zn–rare earth element alloys with long-period stacking ordered phase [J]. Scripta Materialia, 2009, 60: 264–267.
- [32] MOORE M A, DOUTHWAITE R M. Plastic deformation below worn surface [J]. Metallurgical Transactions A, 1976, 7: 1833–1839.
- [33] VENKATARAMAN B, SUNDARARAJAN G. The sliding behaviour of Al–SiC particulate composites II. The characterization of subsurface deformation and correlation with wear behavior [J]. Acta Materialia, 1996, 44: 461–473.

Mg–Gd–Y–Zr 合金在轻微–严重磨损转变状态下的法向载荷与试验温度之间的关系

王渊博¹, 赵伟¹, 李亮¹, 安健^{1,2}

1. 吉林大学 材料科学与工程学院, 长春 130025; 2. 吉林大学 教育部汽车材料重点实验室, 长春 130025

摘要: 研究 Mg–10Gd–1.5Y–0.4Zr 合金的磨损率变化、磨损转变及其与载荷和温度之间的关系。在 20~200 °C 试验温度范围内, 在销盘式试验机上进行磨损试验。磨损表面形貌和成分采用 SEM 和 EDS 方法进行检测。实验结果表明: 在载荷恒定为 20、35 和 40 N 时, 每条磨损率–温度曲线上均会出现一个与轻微–严重磨损转变相对应的转折点。在轻微磨损时, 表层材料因发生塑性变形而产生应变硬化, 而在严重磨损时, 表层材料因发生动态再结晶而发生软化。增加法向载荷将降低轻微–严重磨损转变的临界温度, 法向载荷与发生轻微–严重磨损转变的临界温度之间呈现出近似的线性关系。研究表明: 合金的轻微–严重磨损转变服从表面动态再结晶温度准则。

关键词: Mg–Gd–Y–Zr 合金; 高温磨损; 显微组织; 再结晶; 轻微–严重磨损转变

(Edited by Xiang-qun LI)